Information content per photon versus image fidelity in three-dimensional photon-counting integral imaging

Majeed M. Hayat,[1,*] Srikanth Narravula,[2] Matthew Pepin,[1] and Bahram Javidi[3]

[1]*Center for High Technology Materials and Department of Electrical & Computer Engineering, The University of New Mexico, Albuquerque, New Mexico 87131-1356, USA*
[2]*Department of Physics & Astronomy, The University of New Mexico, Albuquerque, New Mexico 87131-1356, USA*
[3]*Department of Electrical & Computer Engineering, The University of Connecticut, Storrs, Connecticut 06269-2157, USA*
**Corresponding author: hayat@chtm.unm.edu*

Received March 6, 2012; revised August 8, 2012; accepted August 12, 2012;
posted August 13, 2012 (Doc. ID 164021); published September 5, 2012

Photon-counting integral imaging has been introduced recently, and its applications in three-dimensional (3D) object sensing, visualization, recognition, and classification under photon-starved conditions have been demonstrated. This paper sheds light on the underlying information-theoretic foundation behind the ability of photon-counting integral imaging in performing complex tasks with far fewer photons than conventional imaging systems. A metric for photon-information content is formulated in the context of 3D photon-counting imaging, and its properties are investigated. It is shown that there is an inherent trade-off between imaging fidelity, measured by the entropy-normalized mutual information associated with a given imaging system, and the amount of information in each photon used in the imaging process, as represented by the photon-number–normalized mutual information. The dependence of this trade-off on photon statistics, correlation in the 3D image, and the signal-to-noise ratio of the photon-detection system is also investigated.

OCIS codes: 110.3055, 110.0110, 030.5260, 110.3000.

1. INTRODUCTION

Passive three-dimensional (3D) sensing and visualization by 3D computational integral imaging is a method based on the digital implementation of the concept of integral photography [1]. In integral imaging, a series of two-dimensional (2D) elemental images (2D projections) from different perspectives of the 3D scene are recorded. This can be accomplished in a number of ways, such as using a single camera and lenslet array, a camera array, or a single camera on a moving platform [2–14]. Reconstruction may be performed numerically as the reverse of the pickup process by projecting the elemental imaging through a virtual lens array. The advantage of integral imaging over holography or LADAR is that integral imaging can capture 3D color images under ambient or incoherent light illumination. Unlike stereo 3D displays, the 3D integral image can be optically observed without the need for additional viewing devices (or glasses) providing a full parallax autostereoscopic display, which is considered for next-generation 3D TV/display [14]. Thus, an important benefit of integral imaging is the use of mature 2D image capture/display technologies that provide a low-cost implementation with rapid advances in these technologies. Integral imaging has the added advantage of reducing the effects of partial occlusion in the reconstructed scene due to multiple perspectives available during the image capture [14]. In addition, it is possible to relax the constraints on the image pickup stage. That is, the position of image sensors can be randomly distributed in space generating an incoherent synthetic aperture by the distributed sensors. This allows large surveillance scenarios with inexpensive sensors [14].

It has been shown that 3D integral imaging, and, in particular, 3D object recognition with integral imaging under photon-starved conditions can be performed reliably by means of photon-counting integral imaging (PCII) [15–21]. Photon-counting imaging occurs naturally in applications such as astronomy, low-light level imaging, and other electronic systems [22,23]. It could also be used in a variety of pattern recognition systems [24,25].

One of the key benefits of the PCII approach, compared to conventional 3D imaging systems, is that it offers substantial reduction in the number of nonzero pixels required for task-specific sensing and processing. While it is known that sensing based upon detecting individual photons yields the most sensitive photonic imaging possible, what is not presently known is what is the underlying scientific and theoretical foundation of the observed phenomenon with PCII. That is, why imaging with so few photons can perform the complex tasks seen in our PCII experiments. This knowledge can facilitate our understanding of the intricacies of the PCII approach and its performance limits, and help generate a systematic methodology for its optimization. Indeed, the inherent compression in the required photons and captured pixels offered by the PCII approach renders a substantial advantage over conventional methods, making PCII a natural fit to data-intensive 3D applications such as medical imaging, computational imaging, low-light level imaging, homeland security, multi- and hyperspectral imaging, imaging in scattering medium, real-time computation, astronomy, and astrophysics.

To understand the theoretical foundations of PCII 3D imaging systems, there is a need to quantify and understand the concept of information per photon. First of all, let us look into the information-theoretic framework of the imaging system. The object to be imaged is viewed as an information source in the context of information theory whose alphabet is

modeled by a probability distribution function and entropy. The imaging process is modeled as a "communication channel" in which the source alphabet is transformed, in a stochastic fashion, to a formed imaged (output) whose probability distribution is described by the channel conditionally on the input. Now considering the quantum limit of conventional photonic imaging, there is a well-known trade-off between optical energy used to represent a signal, namely the average number of photons per gray level, and the accuracy in the representation of the gray levels. The higher the required fidelity in representing a signal optically, the less informative each individual photon is. The accuracy of an imaging system can be measured by image fidelity of the output image processed through the imaging system. The fidelity of an imaging system should tell us how well the information in an image is preserved by the imaging system. To quantify image fidelity using information theory, we proposed in [19] the fidelity metric, ρ, which is defined as the amount of information we get from an imaging system, normalized by the entropy of the image source. In this paper we further quantify the information carried by each photon in the imaging process by formally introducing here the *photon-information content* metric, I_p, which we define as the mutual information normalized by the number of photons, with the units of bits per photon (bpp).

As a simple example, consider the problem of representing a single pixel with m photons. With m photons, we can represent $m+1$ gray levels, and for the case when the gray levels are evenly spaced and equally likely distributed, we have $\log_2(m+1)$ bits of information [26]. Assuming ideal conditions, without any quantum noise and readout noise, we find that the amount of information we get per photon is $I_p = 2m^{-1}\log_2(m+1)$, since there are $m/2$ photons on an average. With m taking values $1, 2, 3, \ldots\ldots$, the metric I_p forms the sequence 2, 1.58, 1.33, 1.16, ……, and it is easy to check that the maximum value of I_p as a function of m is 2 bpp, attained at $m = 1$. But with just one photon, we will not be able to represent the pixel perfectly. To represent the pixel's true gray level, we would need more photons. Hence, we see a trade-off between the image fidelity and image compression that is inherent in all the imaging systems.

To summarize, in this paper we extend our earlier work [19] so that information per photon is rigorously quantified using information theory and use this concept to quantitatively show the trade-off between imaging quality and information per photon. Moreover, the present paper extends the framework presented in our earlier work to 3D imaging. The remainder of this paper is organized as follows. In Section 2 we give a brief review of the integral imaging system considered in this paper. In Section 3 we present mathematical analysis and derivation of the properties of the photon-information-content metric and provide fundamental upper bounds on this quantity. In Section 4 we study the trade-off between the fidelity metric and the photon-information-content metric and investigate the roles of photon statistics and image correlation on this trade-off. Application of the theory to simulated PCII systems are included in Section 5, and the conclusions are given in Section 6.

2. REVIEW OF INTEGRAL IMAGING

As pointed out earlier, the 3D image can be visualized by recording and processing 2D multiview elemental images that are different perspectives of the 3D object. The elemental images can be captured by a lens array, as depicted in Fig. 1(a), or by moving a single camera with uniform pitch (p). The elemental-image formation step is typically performed by an incoherent optical system and is typically described by a cascade of linear systems, representing degradation factors such as diffraction blur, motion blur, atmospheric turbulence, distortion, etc. However, in this work we assume an ideal imaging system in which the overall impulse response function is approximated as a delta function (namely, the spatial bandwidth of the scene to be imaged is assumed to be much less than the optical bandwidth of the imaging system.) As such, nonoverlapping image samples in each elemental image are assumed independent. (If the finite size of the detector is considered, then the independence assumption remains valid provided that the samples are separated sufficiently so that they image disjoint regions of the object, in which case the samples would be independent.) Moreover, we assume a photon-counting ideal sensor, which counts the photons in each sample (pixel) in the elemental image with detection efficiency η. Noise can also be considered (as in the results in Subsection 3.B), resulting in an error in the photon count.

The 3D images can be reconstructed by a variety of computational reconstruction algorithms [14]. The procedure for computational reconstruction is shown in Fig. 1(b). Each elemental image is projected by magnification $M = z/f$, where z is the distance from the image sensor to the 3D object and f is the focal length of the image sensor, respectively. In order to simplify the computation, we assume that the number of pixels for projected elemental images is the same as the number of pixels for each elemental image. The 3D reconstructed image consists of the sample mean of superimposed pixels. The computational reconstruction algorithm is described as follows:

$$R(x,y,z) = \frac{1}{O(x,y)} \sum_{k=0}^{K-1} \sum_{k=0}^{L-1} I_{kl}(x - kS_x, y - lS_y), \tag{1}$$

with

$$S_x = \frac{N_x p f}{c_x d} \quad \text{and} \quad S_y = \frac{N_y p f}{c_y d}, \tag{2}$$

where x, y are the index of pixels in the x and y directions, respectively; N_x and N_y are the number of pixels for each elemental image in x and y directions, respectively; p is the moving pitch between image sensors; c_x and c_y are the size of the image sensor in the x and y directions, respectively; S_x and S_y are the number of shifted pixels for superposition in x and y directions, respectively; I_{kl} is the intensity of the kth column and lth row elemental image; $O(x,y)$ is the overlapping number matrix; and $R(x,y,z)$ is the intensity of the reconstructed 3D image.

3. INFORMATION-THEORETIC MODEL FOR 3D PHOTON-COUNTING IMAGING

Any imaging system, and in particular a photon-counting imaging system, can be viewed as a communication-theoretic system, as shown in Fig. 2. Following our recent foundational work [19] on 2D photon-counting imaging systems, the "source" or "input" is the ensemble of all possible (true)

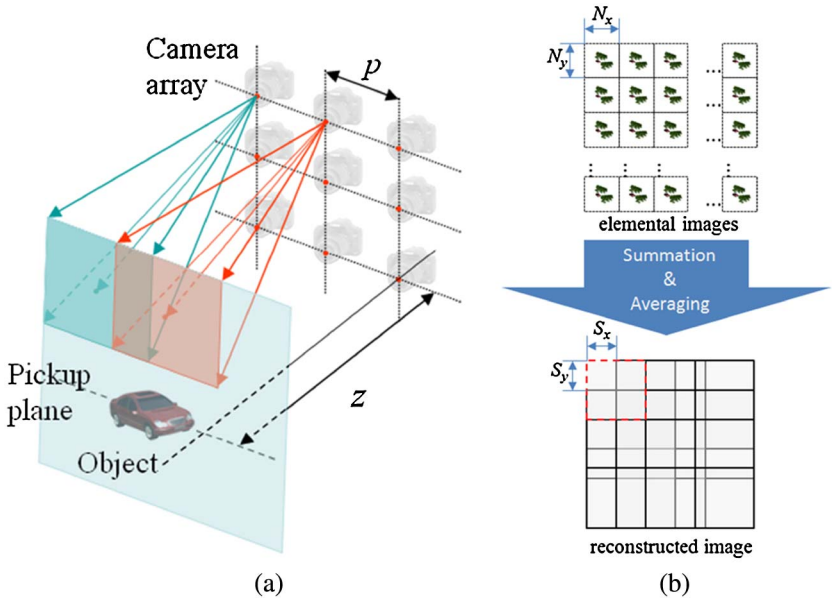

Fig. 1. (Color online) 3D integral imaging. (a) Pickup (image capture) stage (passive sensing), (b) computational image reconstruction.

intensity images of interest; the "channel" represents a stochastic transformation that maps each intensity image to a stochastic spatio-temporal point process representing the often-weak photon stream, followed by a photon-counting system; and the "output" is the array of photon-counts that constitutes the reconstructed image. Under Poisson photon statistics, conditioned on the irradiance image, the output is characterized by the received photon-flux density and the photon-detection system. The stochastic photon streams considered in a PCII system typically undergo severe random deletions (or thinning) of photons due to absorption and scattering in the transmission medium. The total photon count in the photon-counting array represents a degraded version of the source image.

Mathematically, consider a stochastic column vector $\mathbf{X}$ whose entries, X_i, $i = 1, \ldots, n$, are discrete random variables in the interval [0, 1] representing the reflectance of some unknown object or an unknown digital image. Note that we are considering X_i to be a discrete random variable as opposed to a continuous one to simplify our calculations of entropy and mutual information. The ith element of the detector array gives a measurement of the number of photons, Y_i, detected during integration time τ. For a Poisson photon statistics and conditional on a particular realization of the true intensity X_i, say $X_i = x_i$, the count Y_i is a Poisson random variable with mean value $x_i \epsilon N_p$, where $N_p = \eta\lambda\tau$ is the mean number of photons per pixel and per unit integration time τ, η is the quantum efficiency of the detector, λ is the photon flux of the unattenuated light, and ϵ is the probability that a source photon is not scattered as it is transmitted. Therefore, the *conditional* probability mass function of Y_i given that $X_i = x_i$ can be written as

$$P_{Y_i|X_i}(y_i|x_i) = \frac{(N_p x_i \epsilon)^{y_i} e^{-N_p x_i \epsilon}}{y_i!}, \qquad y_i = 0, 1, 2, \ldots. \tag{3}$$

We define the photon-count image, $\mathbf{Y}$, as a stochastic array whose entries are the integer-valued random variables Y_i; this stochastic array represents the photon-count array (2D or 3D). Under the assumption that the output pixels are independent conditional on the input $\mathbf{X}$, the conditional probability mass function of the output $\mathbf{Y}$ is given by $P_{\mathbf{Y}|\mathbf{X}}(\mathbf{y}|\mathbf{x}) = \Pi_{i=1}^{n} P_{Y_i|X_i}(y_i|x_i)$, and the probability mass function of the output is $P_{\mathbf{Y}}(\mathbf{y}) = \sum_{\mathbf{x}} P_{\mathbf{Y}|\mathbf{X}}(\mathbf{y}|\mathbf{x}) P_{\mathbf{X}}(\mathbf{x})$, where $P_{\mathbf{X}}(\cdot)$ is the probability mass function of the source image $\mathbf{X}$, and the summation is over all realizations $\mathbf{x}$ of $\mathbf{X}$ [19].

In [19] we introduced the normalized mutual information metric, or image-fidelity metric denoted by ρ, as $\rho = I(\mathbf{Y};\mathbf{X})/H(\mathbf{X})$, where $H(\mathbf{X}) = -\mathsf{E}[\log_2(P_{\mathbf{X}}(\mathbf{X}))] = \sum_{\mathbf{x}} \log_2(1/P_{\mathbf{X}}(\mathbf{x})) P_{\mathbf{X}}(\mathbf{x})$ is the entropy of the input image and $I(\mathbf{Y};\mathbf{X}) = \mathsf{E}[\log_2(P_{\mathbf{Y}|\mathbf{X}}(\mathbf{Y}|\mathbf{X})/P_{\mathbf{Y}}(\mathbf{Y}))] = \sum_{\mathbf{x},\mathbf{y}} \log_2(P_{\mathbf{Y}|\mathbf{X}}(\mathbf{y}|\mathbf{x})/P_{\mathbf{Y}}(\mathbf{y})) P_{\mathbf{X},\mathbf{Y}}(\mathbf{x},\mathbf{y})$ is the mutual information between the output and input images, $P_{\mathbf{X},\mathbf{Y}}(\mathbf{x},\mathbf{y}) = P_{\mathbf{Y}|\mathbf{X}}(\mathbf{y}|\mathbf{x}) P_{\mathbf{X}}(\mathbf{x})$, and $\mathsf{E}[\cdot]$ is the

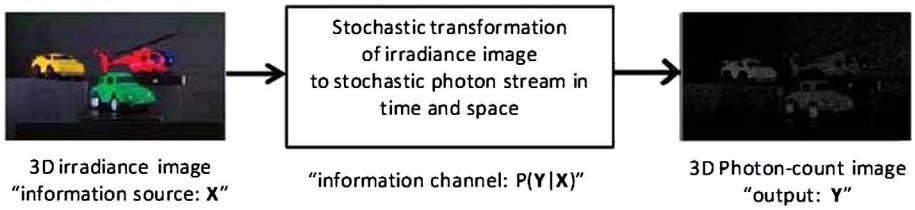

Fig. 2. (Color online) Information-theoretic representation of a photon-counting imaging system. Photons from the input scene pass through the medium, resulting in a photon-starved stochastic photon stream in time and space. Photons are detected by a photon-counting array yielding output image with M gray levels. At extremely low photon numbers, as is typically the case with the PCII approach, the output image is a very sparse, binary image.

usual notation for the expected value of a random variable/vector. Note that $0 \le \rho \le 1$ since the mutual information is always upper bounded by the entropy, with equality to unity when the input $\mathbf{X}$ can be retrieved exactly (without ambiguity) from the output Y, while ρ is zero when $\mathbf{X}$ and $\mathbf{Y}$ are statistically independent [26]. We next extend the framework to include depth dimension, which, in turn, enables us to extend the fidelity metric to 3D and also define the 3D photon-information-content metric.

Consider the sequence of input 2D images, $\mathbf{X}^{(1)}, \ldots..., \mathbf{X}^{(L)}$, corresponding to the depths $z_1, \ldots..., z_L$, and let $\mathbf{Y}^{(1)}, \ldots..., \mathbf{Y}^{(L)}$ denote the photon-count images at the output resulting from processing the elemental images according to the PCII method [15]. Using the convenient expectation notation, the entropy of the 3D input image is defined as

$$H(\mathbf{X}^{(L)}, \ldots \mathbf{X}^{(1)}) \triangleq - \mathsf{E}[\log_2(P_{\mathbf{X}^{(L)},\ldots\mathbf{X}^{(1)}}(\mathbf{X}^{(L)}, \ldots, \mathbf{X}^{(1)}))], \quad (4)$$

and the mutual information between the 3D input and output is

$$I(\mathbf{Y}^{(L)}, \ldots, \mathbf{Y}^{(1)}; \mathbf{X}^{(L)}, \ldots, \mathbf{X}^{(1)}) \triangleq \mathsf{E}\left[\log_2\left(\frac{P_{\mathbf{Y}^{(L)},\ldots,\mathbf{Y}^{(1)}|\mathbf{X}^{(L)},\ldots,\mathbf{X}^{(1)}}(\mathbf{Y}^{(L)}, \ldots, \mathbf{Y}^{(1)}|\mathbf{X}^{(L)}, \ldots, \mathbf{X}^{(1)})}{P_{\mathbf{Y}^{(L)},\ldots,\mathbf{Y}^{(1)}}(\mathbf{Y}^{(L)}, \ldots, \mathbf{Y}^{(1)})}\right)\right]. \quad (5)$$

Now the 3D fidelity metric is then defined as the ratio

$$\rho \triangleq \frac{I(\mathbf{Y}^{(L)}, \ldots \mathbf{Y}^{(1)}; \mathbf{X}^{(L)}, \ldots, \mathbf{X}^{(1)})}{H(\mathbf{X}^{(L)}, \ldots, \mathbf{X}^{(1)})}, \quad (6)$$

so that the fidelity metric, ρ, is upper bounded by unity. Next, with the mutual information of a 3D image at hand, the photon-information-content metric, I_p, can be defined as

$$I_p = I(\mathbf{Y}^{(L)}, \ldots, \mathbf{Y}^{(1)}; \mathbf{X}^{(L)}, \ldots, \mathbf{X}^{(1)})/m, \quad (7)$$

where m is the mean number of photons per image.

A. Fundamental Bounds on the Photon-Information-Content Metric

As we have seen in Section 1 for a binary single-pixel image and assuming ideal imaging, the photon-information metric is at its maximum value of 2 bpp when we use a single photon to represent "1" and no photons to represent "0" with equal probability. By extending the single-pixel model, we will be able to find bounds on the photon-information-content metric, I_p, for any ideal imaging system and for several classes of photon-starved images. If we include quantum noise and readout noise, as done in Subsection 3.B, the photon-information metric is lowered accordingly.

Under ideal conditions, the random vector $\mathbf{Y}$ is simply the source $\mathbf{X}$ (or more precisely, $\mathbf{Y}$ would be a 1-1 deterministic transformation of $\mathbf{X}$). As such, the mutual information $I(\mathbf{Y};\mathbf{X})$ is simply the entropy $H(\mathbf{X})$. First, consider the class of binary n-pixel (2D or 3D) images that have at most only one nonzero pixel. Assuming ideal imaging conditions, we would need only one photon to represent such an image. Since we can have a total of $n+1$ possible images (including the all-zero image), the maximum entropy of the image (when all $n+1$ possibilities occur with equal probability) is $\log_2(n+1)$. Now the average number of photons in any one of the $n+1$ images is $n/(n+1)$; therefore, the maximum of the photon-information-content metric in this case is simply $I_p = (1+n^{-1})\log_2(n+1)$ bpp. As expected, when in the single-pixel case ($n=1$), $I_p = 2$ bpp.

Next, consider the class of binary n-pixels images that have zero entries at all sites except at exactly k nonzero sites ($k = 1, \ldots..., n$) with at most one photon per pixel. Here, there are $\binom{n}{k}+1$ equally likely possible images, including the all-zero image. Note that in this case the average number of photons is $n_k = k/(1+\binom{n}{k}^{-1})$. Therefore, the photon-information-content metric is given by

$$\begin{aligned} I_p &= \frac{\log_2\left(\binom{n}{k}+1\right)}{n_k} \le \frac{\log_2\left(\binom{n+1}{k}\right)}{n_k} \\ &= \frac{\log_2(n+1)+\cdots+\log_2(n-k+2)-\log_2(k!)}{n_k} \\ &\le \left(1+\binom{n}{k}^{-1}\right)\log_2(n+1), \end{aligned} \quad (8)$$

which shows that I_p is at a maximum value of $(1+n^{-1})\log_2(n+1)$ when $k=1$.

Generalizing the above reasoning (ignoring the all-zero case for simplicity), any photon-count image with m total photons in k pixels can be thought as distributing m photons in k bins taken from n bins (assuming $k \le n$). Since there are $\binom{n}{k}$ ways to select the k bins and since for each arrangement of the k bins we can distribute the m photons in $\binom{m-1}{k-1}$ ways so that no bin is left empty (assuming $k \le m$), there are $\binom{n}{k}\binom{m-1}{k-1}$ such distributions or images. Thus, $I_p = m^{-1}\log_2(\binom{n}{k}\binom{m-1}{k-1})$, which can be shown to be upper bounded by $\log_2(n)$ whenever $m \le n$ and $k \le n/2$, namely when the image has a low number of photons.

In summary, for any n-pixel, photon-starved count image, where n is large, I_p is upper bounded approximately by $\log_2(n)$, and the highest value occurs when only one photon per image is utilized.

B. Trade-off Between Photon-Information Content and Fidelity Metric: Single-Pixel Case

When uncertainty in the imaging system is present, then increasing the number of photons can improve the photon-information content as it works to combat the degrading effects brought about by uncertainty. However, there will be a point of diminishing returns when the increase in the mutual information (as in the fidelity metric) plateaus, and adding more photons can be redundant and therefore wasteful. The results shown in this subsection establish this trade-off for a single pixel.

Consider a binary photon-counting system ($M=2$) for a single pixel, depicted in Fig. 3. There are three sources of uncertainty in this example: (1) quantum noise (statistical uncertainty in the actual number of detected photons corresponding to gray levels), (2) additive dark current and readout noise from the detector that can also contribute to false counts, and (3) nonideal quantum efficiency of the detector, which results in random misses in the counting process. The channel probabilities are calculated as follows. We assume

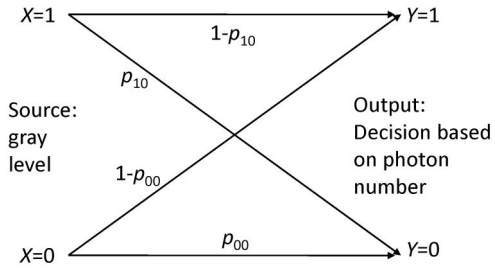

Fig. 3. Binary asymmetric channel representing the transformation of a gray level to a maximum-likelihood decision based upon photon numbers in quantum and dark/readout noise.

that the equally likely gray levels of 0 and 1 result in photon numbers 0 and m, respectively, where m is used as a free parameter representing the intensity of the "1" level. A decision threshold of $\eta m/2$ is then used to convert the counts to binary gray levels, where as before, η is the detector's quantum efficiency. (Note that the effects of scattering of photons can be lumped with the quantum efficiency.) In the absence of dark/readout noise, a Poisson model is used and the calculated transition probabilities are $p_{00}=1$, $p_{01}=0$, $p_{10}=e^{-\eta m}$, and $p_{11}=1-p_{10}$. On the other hand, when dark/readout noise is present, a Gaussian approximation is used to calculate the error probabilities. The results are $p_{00}=0.5\left(1+\mathrm{erf}\left(\frac{\eta m}{2\sqrt{2}\sigma}\right)\right)$ and $p_{10}=0.5\left(1-\mathrm{erf}\left(\frac{\eta m}{2\sqrt{2(\eta m+\sigma^2)}}\right)\right)$, where σ^2 is the variance of the noise and $\mathrm{erf}(x)=\frac{2}{\sqrt{\pi}}\int_0^x e^{-t^2}\mathrm{d}t$.

We have calculated the photon-information-content metric, I_p, and obtained the graph in Fig. 4. In particular, in the quantum-noise limit ($\sigma=0$, $\eta=1$), I_p assumes its peak value of about 1.44 bpp in the limit as $m\to 0$, which is about 72% of the maximum value in the ideal case (recall that $I_p=2$ bpp in the ideal single-pixel case); this reduction is due to quantum noise. The 10*e* noise example shown corresponds to the state-of-the-art p-i-n detector. It is interesting to see the trend in these graphs. Namely, depending on the imaging-system parameters [represented by the system's signal-to-noise ratio (SNR)], there is an optimal value for the average number of photons per gray level required in the transmission process for which the metric I_p is maximized. This maximizing average photon number corresponds to a fair balance in reducing the role of uncertainty (due to the finite SNR associated with the photon-counting imaging process) without wasting photons. However, maximizing the photon-information content alone by making the photons rare may not be desirable, despite the fact that photons are efficient. This is because the information conveyed by the rare photons, measured by the fidelity metric, can be small as shown in Fig. 5, which shows the calculated fidelity metric, ρ. The fidelity metric increases monotonically with m, and in particular and in the quantum-noise limit, ρ approaches its peak value of 1 in the limit as $m\to\infty$.

The results shown in this section show the trade-off between the metrics I_p and ρ. The generalization of these results to 3D images is considered next.

4. TRADE-OFF BETWEEN FIDELITY METRIC AND PHOTON-INFORMATION-CONTENT METRIC IN 3D IMAGES

We begin by examining the dependence of each of the fidelity and photon-information-content metrics on the number of photons per pixel in 3D images. To do so, we generate ensembles of 3D images, $\mathbf{X}$, using a 3D Markov-random field (MRF) distribution and simulate the photon-counting imaging system to produce the photon-count images $\mathbf{Y}$ for various scenarios of the mean photon number per image. Once the pair of the source image $\mathbf{X}$ and the photon-count image $\mathbf{Y}$ are available, we estimate $H(\mathbf{X})$ and $I(\mathbf{Y};\mathbf{X})$ for the neighborhood of every pixel [27], which is known to be proportional to $H(\mathbf{X})$ and $I(\mathbf{Y};\mathbf{X})$ for the image. These estimates are then improved by averaging over multiple realizations of $\mathbf{X}$ and $\mathbf{Y}$. The metrics I_p and ρ are then computed from the estimates of $H(\mathbf{X})$ and $I(\mathbf{Y};\mathbf{X})$.

Here, we use a 3D version of the model used in [19] to generate ensembles of 3D images with controlled correlation properties. A generalized 3D Ising MRF model is characterized by its 3D-clique potential function. A collection of sites is said to be a clique if every two sites in it are considered neighbors based on some predefined association rule; hence, all one-site sets are automatically cliques. The 3D Ising potential function has the following form:

$$V_c(\mathbf{X})=\begin{cases}\beta_c & \text{if the pixel values of } \mathbf{X} \text{ at the sites in } c \text{ are the same}\\ -\beta_c & \text{otherwise,}\end{cases} \tag{9}$$

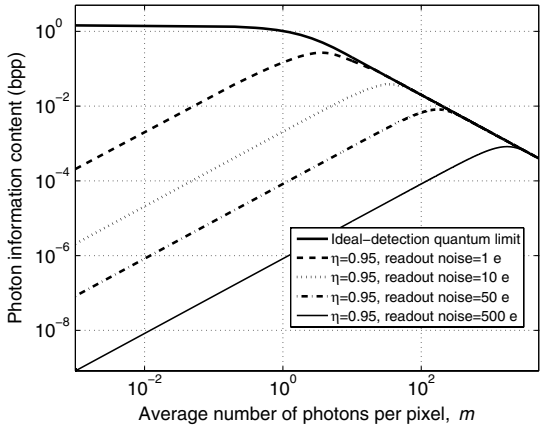

Fig. 4. Photon-information-content metric, I_p (in bpp), versus average number of photons for various levels of quantum efficiency and dark/readout noise.

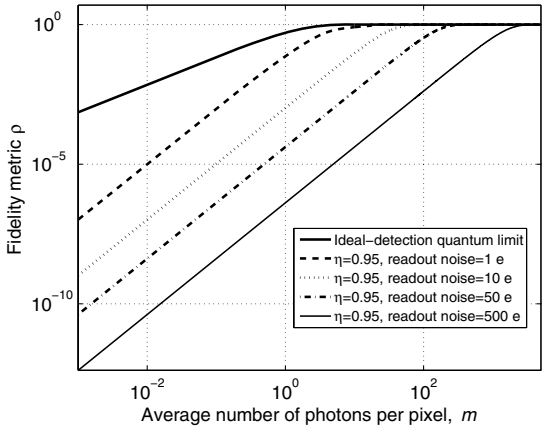

Fig. 5. Fidelity metric, ρ, versus average number of photons for various levels of quantum efficiency and dark/readout noise.

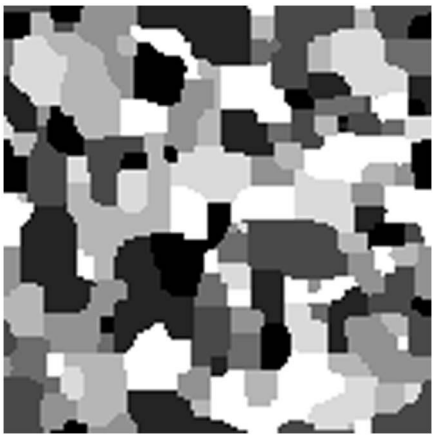

Fig. 6. 2D slice of the a 3D Ising MRF realization exhibiting strong correlation. The correlation structure is symmetric in x, y, and z directions. The 3D MRF described in the text was used to generate the 3D images assuming $\beta_c = 0.6$.

where β_c is a real number dependent on the clique and it controls the 3D correlation in the image. In our simulations, we have used the following notion of site neighborhood: two sites are neighbors if they are adjacent in horizontal, vertical, or depth directions. The specification of the parameter β_c is given as follows: for any one-site clique c, $\beta_c = 1$; for any two-site clique, $\beta_c = \beta$, a constant. Finally, for all three-site cliques and higher, $\beta_c = 0$. We followed the Metropolis sampling algorithm [28] to generate 3 bit (8 gray levels) 3D images of size $128 \times 128 \times 8$ with β varied at will to control the 3D correlation. (As in [19], the temperature parameter in the Ising model was set to 3.) The algorithm is run for 1000 iterations for each image generated; an example is shown in Fig. 6.

Figures 7 and 8 show the dependence of the metrics I_p and ρ on the mean number of photons per pixel for three cases of correlation: (1) images with no correlation in any dimension, (2) images with only spatial correlation (in two dimensions) for each depth while the 2D images from different depths are uncorrelated, and (3) images with full 3D correlation. In simulating images for case 1, the pixel values are assumed independent. For case 3, the 3D MRF described above was used with

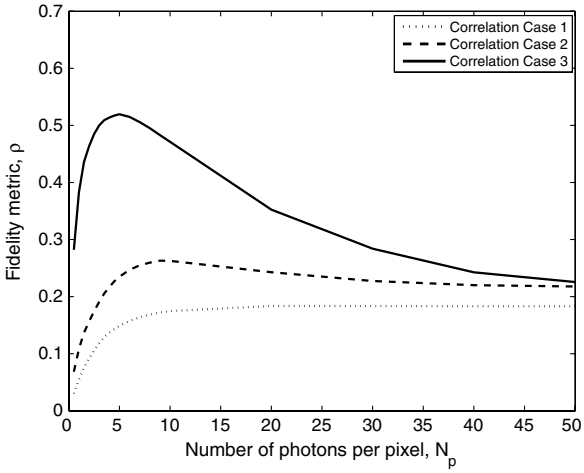

Fig. 7. Fidelity metric as a function of the average number of photons per pixel for three scenarios of correlation: no correlation (case 1), only 2D correlation in the $x-y$ plane (case 2), and full 3D correlation (case 3).

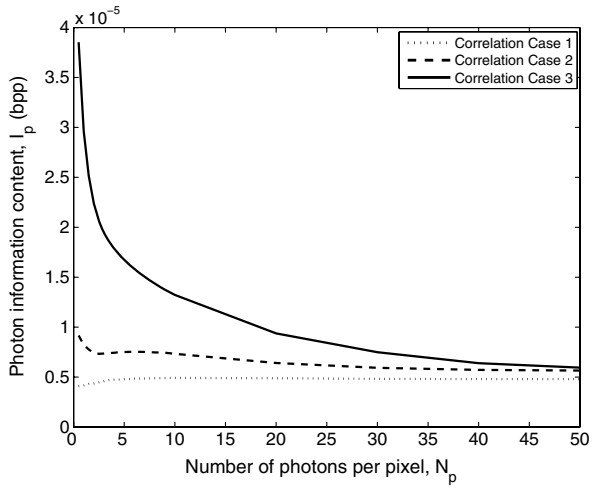

Fig. 8. Photon-information-content metric as a function of the average number of photons per pixel for three scenarios of correlation: no correlation (case 1), only 2D correlation in the $x-y$ plane (case 2), and full 3D correlation (case 3).

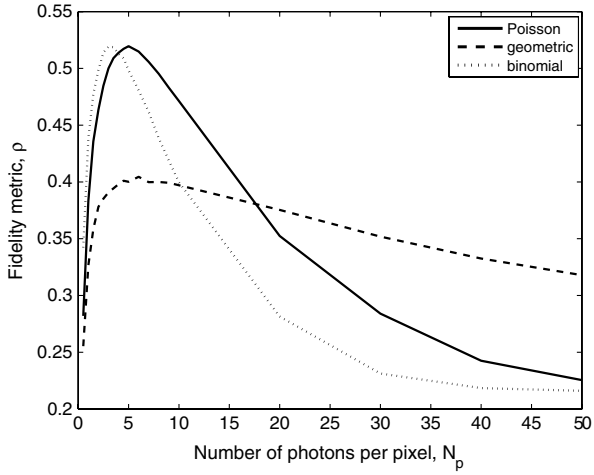

Fig. 9. Fidelity metric as a function of the average number of photons per pixel for three different photon statistics: Poisson, geometric, and binomial.

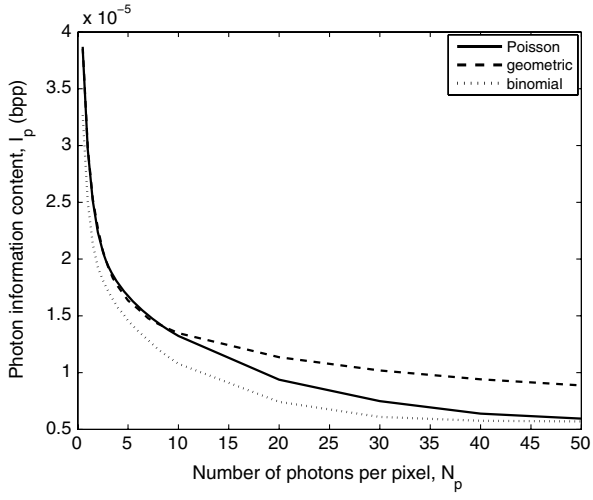

Fig. 10. Photon-information-content metric as a function of the average number of photons per pixel for three different photon statistics: Poisson, geometric, and binomial.

(a)

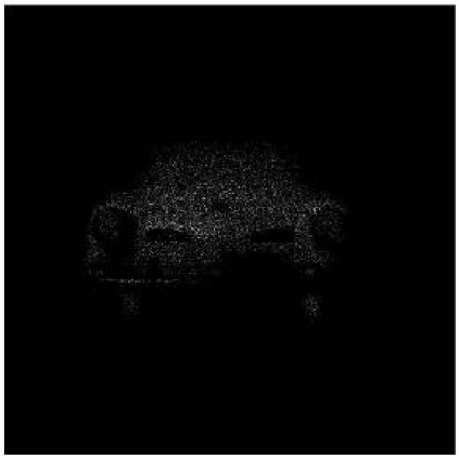

(b)

Fig. 11. (Color online) Input 500×500 image (a) and one slice [at 370 mm] of the 3D reconstruction (b) using the PCII system. The calculated fidelity metric is $\rho = 0.2438$ and $I_p = 0.86$ bpp. The mutual information and entropy are estimated as in [19].

$\beta_c = 0.6$. To simulate images with only 2D correlation similar to the correlation present in the 3D image, as in case 2, we formed a 3D image by taking a depth slice from different realizations of the 3D MRF image. In this fashion the spatial correlation in the $x-y$ plane of the 3D MRF realization is kept intact, but the depth correlation (along the z axis) is destroyed. It is seen that the highest fidelity metric is obtained when 3D correlation is present, as in case 3. In contrast, the independent-pixel case exhibits the lowest value of ρ. The connection between correlation and the image-fidelity metric was made first in 2D images [19]: the presence of spatial correlation leads to higher values of the fidelity metric. Here, we see that the added correlation in the depth dimension causes further increase in the fidelity metric. As for the dependence of the fidelity metric on the average number of photons per pixel, N_p, we see that ρ increases with N_p up to a point, after which it drops monotonically, as seen in Fig. 7. The initial increase in ρ is expected as higher N_p results in less uncertainty in the photon-count image as the role of quantum noise and scattering is reduced. However, the eventual decrease is due to gray-level truncation; namely, the photon-count image gray levels are limited to 0 and 1 in these simulations, where all nonzero counts are lumped together as a generic "1" count. To see the reason behind such drop in the fidelity metric, note that for any fixed level of truncation (or quantization) of the output count, the fidelity metric converges to zero as the mean number of photons per pixel, N_p, tends to infinity. More precisely, for a given level of thresholding, as N_p increases the probability mass function of the truncated output becomes concentrated at the highest quantized level (approaching a delta function). Hence, the entropy of the truncated output will converge to zero as N_p tends to infinity, and so does the mutual information since it is upper bounded by the entropy of the truncated output.

As for the information content per photon, we see a similar trend in terms of correlation. In general, I_p is higher in 3D images that have a high degree of correlation, especially correlation in the depth direction, as seen in Fig. 8. Moreover, I_p decreases with N_p as the benefit in having more photons (in reducing uncertainty in the photon-count image) is outweighed by the redundancy of having more photons.

A. Role of Photon Statistics

Next, we investigate the effect of photon statistics on the metrics ρ and I_p. Figure 9 shows the fidelity metric ρ when the photon statistics follow binomial and Boltzmann (geometric) distributions. In the former case, the probability mass function of Y_i conditional on X_i is binomial, and in the latter case the probability mass function is geometric; more details on these distributions in the context of photon-counting imaging are available in [19]. The binomial model is suitable in modeling photon statistics of nonclassical light when the probing light is maximally amplitude squeezed [29]. An amplitude-squeezed state can result in narrowing the distribution of the photon

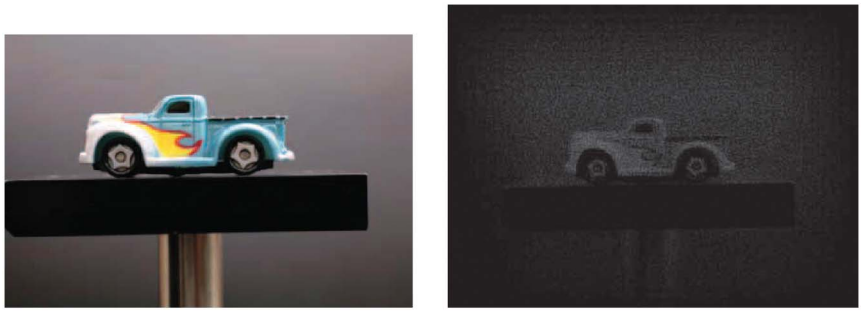

(a) (b)

Fig. 12. (Color online) (a) Input (true) 1664×2496 image used to generate 100 elemental images (with an average of 10 000 photons in each elemental image) and 3D reconstruction based on PCII and (b) one slice at 95 mm.

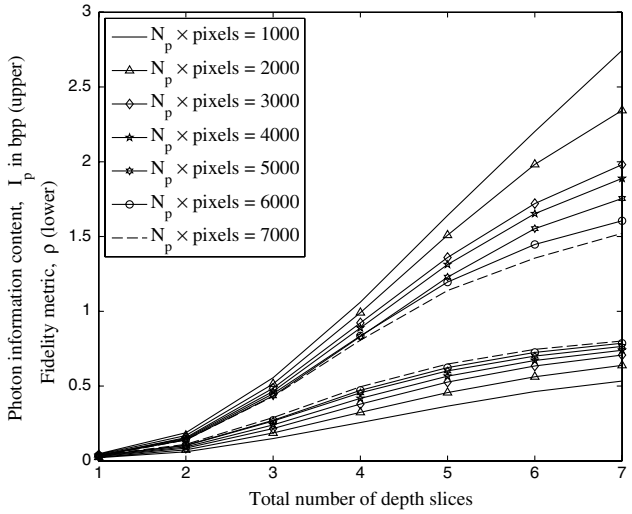

Fig. 13. Fidelity metric and photon-information content versus number of depth slices used (256 gray levels). The reconstruction was performed using 100 elemental images with each elemental image having, on average, $N_p \times 1664 \times 2496$ photons.

number, viz., reducing the photon-number uncertainty and hence reducing quantum noise below the classical shot-noise limit (associated with light with Poisson photon statistics). The geometric distribution is suitable for modeling, for example, the photon statistics of thermal light, and it has higher photon-number uncertainty compared to Poissonian light [30]. For comparison, the results corresponding to the Poisson statistics are also overlayed. For consistency, we have assumed the same mean value for all three distributions. We find that for small values of the mean photon number per pixel ($N_p < 4$), Poisson photon statistics yield a higher fidelity metric than that for the Boltzmann photon statistics but lower than that for the binomial distribution. This is because uncertainty in the photon number is higher in the Boltzmann photon statistics than that for Poisson statistics, and the opposite is true for the binomial photon statistics. A reduced (increased) quantum noise compared to the Poisson-statistics case implies that the photon count resembles the image more closely (remotely), in turn implying higher (lower) correlation between the source image and the photon-counting output image. For I_p, it is seen from Fig. 10 that for low photon counts N_p, the binomial photon statistics yield smaller I_p than those for the Poisson and Boltzmann statistics; this is because the binomial distribution has less photon-number uncertainty and hence less net mutual information, unless normalized by the entropy as in the case of ρ, where we found that ρ was higher for the binomial statistics than those for the other two.

5. APPLICATION TO SIMULATED 3D PCII IMAGERY

To put the results of Section 4 in the context of PCII, we have generated simulations of the 3D reconstruction of a real 3D object using the PCII approach and empirically calculated the metrics I_p and ρ. We begin by considering I_p for a representative quantum-noise limited example shown in Fig. 11(a). We have calculated $I_p = 0.86$ bpp and $\rho = 0.2438$ for the 8 bit 2D projection, shown in Fig. 11(b), of the 3D reconstruction by means of the PCII method [21]. The reconstruction is obtained from a set of 100 elemental images (with resolution 500×500 pixel), with 21 618 photons in total in all the

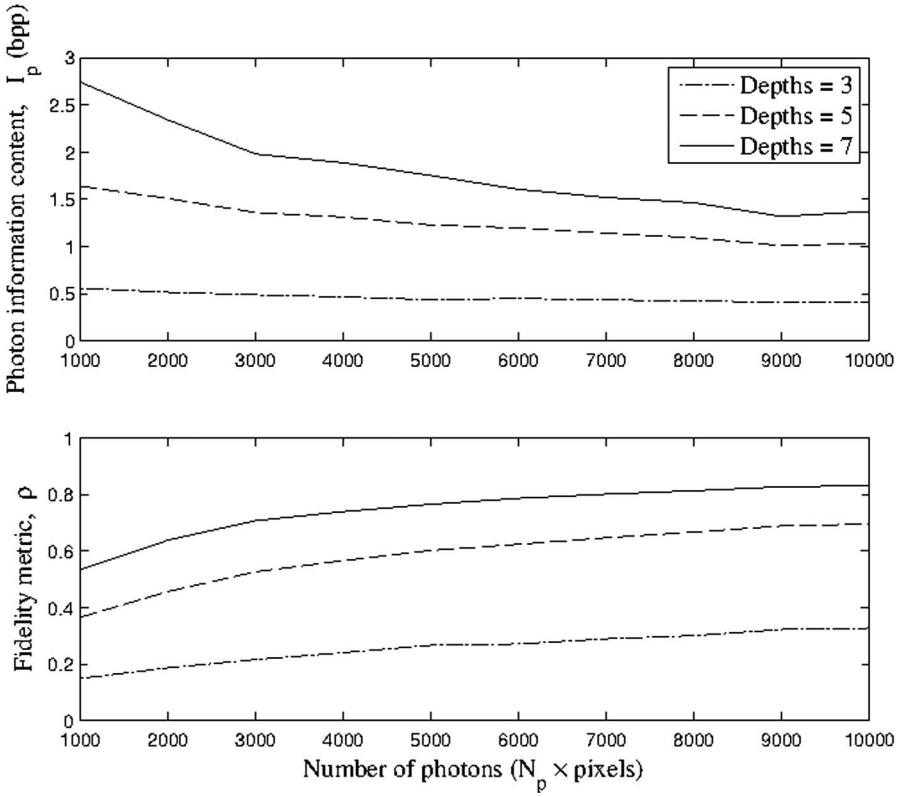

Fig. 14. Fidelity metric and photon-information content versus number of photons per pixel for different number of depths included in the 3D image (256 gray levels).

Table 1. Fidelity Metric (ρ) Versus Photon-Information-Content Metric (I_p) for a Representative Elemental Image (EI) and the Reconstructed Image (RI)

Image type	I_p (bpp)	ρ
EI	0.9895	0.0150
RI	0.5636	0.4535

elemental images. (The entropy and mutual information were estimated using the Ising MRF method used in [19].)

We also determined the effect of using more depth information on I_p and ρ in 3D reconstructions from a fixed number of elemental images. In this case, ρ and I_p were calculated from a multidimensional histogram with up to seven dimensions (one per depth) and the photon counts in all 10 000 1664×2496 elemental images. In the PCII, data volume depths ranged from 90 to 120 mm and the average number of photons per elemental image, $N_p \times 1664 \times 2496$, varied between 1000 and 10 000 photons per elemental image. The true object that was imaged is shown in Fig. 12(a) and a slice of its 3D reconstruction is shown in Fig. 12(b). We investigated the role of including depth information progressively as we consider more and more depth layers. As expected and as seen in Fig. 13, as we include more slices of the 3D volume, the cumulative bpp increases. This will eventually converge to the I_p for the entire 3D image cube. To see the trade-off between I_p and ρ in a 3D setting, we plot these metrics in Fig. 14 as a function of N_p for different sizes of the reconstructed 3D image, namely for the cases when 3, 5, and 7 depths are used. The trade-off in I_p and ρ is clear.

Finally, we make the observation that as seen in Table 1, the photon-information content is very high for elemental images whereas the fidelity is very low. In contrast, for the reconstructed images, the image fidelity is very high but the photon-information content is low.

6. CONCLUSIONS

We have introduced an information-theoretic metric, termed the photon-information content, that measures the amount of Shannon's information each photon provides in 3D photon-counting imaging systems. This metric, in conjunction with the entropy-normalized mutual information for image fidelity in photon-counting imaging systems, together provide a means of assessment and trade-off analysis between quality of imaging and conservation in photon usage, or photon-number compression. The trade-off between photon-number compression and image quality was investigated in 3D images both in the context of photon-counting imaging and PCII. The role of 3D correlation (especially in the depth dimension) as well as the photon statistics were investigated.

Not only is assessment and optimization of photon-counting imaging and photon-counting integral imaging possible through these metrics, but they are also applicable to a much larger realm of existing and potential information-transmission driven systems. The limits of such systems in terms of photon-number compression and fidelity play directly to the requirements placed upon these systems to convey as much information as possible in a limited time and to enable decisions at the earliest possible time from the available data. For example, in the context of automatic target recognition, with maximal photon-number compression subject to a prescribed fidelity constraint, an ideal identification image/object template can be realized optimally, thus streamlining the optical identification process. The performance bounds of image identification can then be assessed independently of the transmission channel and its noise with a more thorough understanding of the information-degradation process involved in the imaging process. Extension is possible to other 3D passive sensing paradigms, multiview photon-counting imaging, multidata (hyperspectral or gamma ray) imaging, or even sparse-sensor arrangements.

ACKNOWLEDGMENTS

The authors wish to acknowledge Myungjin Cho for generating the integral imaging data. B. Javidi acknowledges Defense Advanced Research Projects Agency (DARPA) support under contract FA8650-09-C-7934.

REFERENCES

1. G. Lippmann, "Epreuves reversibles donnant la sensation du relief," J. Phys. (Paris) **7**, 821–825 (1908).
2. C. B. Burckhardt, "Optimum parameters and resolution limitation of integral photography," J. Opt. Soc. Am. A **58**, 71–76 (1968).
3. T. Okoshi, "Three-dimensional displays," Proc. IEEE **68**, 548–564 (1980).
4. H. Hoshino, F. Okano, H. Isono, and I. Yuyama, "Analysis of resolution limitation of integral photography," J. Opt. Soc. Am. A **15**, 2059–2065 (1998).
5. A. Stern and B. Javidi, "Three-dimensional image sensing, visualization, and processing using integral imaging," Proc. IEEE **94**, 591–607 (2006).
6. R. Martinez-Cuenca, G. Saavedra, M. Martinez-Corral, and B. Javidi, "Progress in 3-d multiperspective display by integral imaging," J. Opt. Soc. Am. A **20**, 411–420 (2003).
7. M. C. Forman, N. Davies, and M. McCormick, "Continuous parallax in discrete pixelated integral three-dimensional displays," Proc. IEEE **97**, 1067–1077 (2009).
8. F. Okano, J. Arai, K. Mitani, and M. Okui, "Real-time integral imaging based on extremely high resolution video system," Proc. IEEE **94**, 490–501 (2006).
9. B. Javidi, F. Okano, and J. Y. Son, eds., *Three Dimensional Imaging, Visualization, and Display*" (Springer, 2008).
10. B. Javidi, S.-H. Hong, and O. Matoba, "Multi dimensional optical sensors and imaging systems," Appl. Opt. **45**, 2986–2994 (2006).
11. H. E. Ives, "Optical properties of a lippmann lenticulated sheet," J. Opt. Soc. Am. A **21**, 171–176 (1931).
12. H. Arimoto and B. Javidi, "Integrated three-dimensional imaging with computed reconstruction," Opt. Lett. **26**, 157–159 (2001).
13. J. S. Jang and B. Javidi, "3D synthetic aperture integral imaging," Opt. Lett. **27**, 1144–1146 (2002).
14. M. Cho, M. Daneshpanah, I. Moon, and B. Javidi, "Three-dimensional optical sensing and visualization using integral imaging," Proc. IEEE **99**, 556–575 (2011).
15. B. Tavakoli, B. Javidi, and E. Watson, "Three-dimensional visualization by photon counting computational integral imaging," Opt. Express **16**, 4426–4436 (2008).
16. I. Moon and B. Javidi, "Three-dimensional recognition of photon starved events using computational integral imaging and statistical sampling," Opt. Lett. **34**, 731–733 (2009).
17. S. Yeom, B. Javidi, and E. Watson, "Three-dimensional distortion-tolerant object recognition using photon-counting integral imaging," Opt. Express **15**, 1513–1533 (2007).
18. S. Yeom, B. Javidi, and E. Watson, "Photon counting passive 3D image sensing for automatic target recognition," Opt. Express **13**, 9310–9330 (2005).
19. S. R. Narravula, M. M. Hayat, and B. Javidi, "Information theoretic approach for assessing image fidelity in photon-counting arrays," Opt. Express **18**, 2449–2466 (2010).

20. S. Yeom, B. Javidi, C. Lee, and E. A. Watson, "Photon-counting passive 3D image sensing for reconstruction and recognition of occluded objects," Opt. Express **15**, 16189–16195 (2007).
21. D. Dey, J. Jung, M. Cho, and B. Javidi, "Three-dimensional photon counting integral imaging using Bayesian estimation," Opt. Lett. **35**, 1825–1827 (2010).
22. M. Guillaume, P. Melon, and P. Refregier, "Maximum-likelihood estimation of an astronomical image from a sequence at low photon levels," J. Opt. Soc. Am. A **15**, 2841–2848 (1998).
23. D. Stucki, G. Ribordy, A. Stefanov, H. Zbinden, J. G. Rarity, and T. Wall, "Photon counting for quantum key distribution with Peltier cooled InGaAs/InP APDs," J. Mod. Opt. **48**, 1967–1981 (2001).
24. F. Sadjadi, Selected papers on automatic target recognition, SPIE-CDROM (1999).
25. A. Mahalanobis and R. Muise, "Object specific image reconstruction using a compressive sensing architecture for application in surveillance," IEEE Trans. Aerospace Electron. Syst. **45**, 1167–1180 (2009).
26. T. M. Cover and J. A. Thomas, *Elements of Information Theory* (Wiley, 1991).
27. E. Volden, G. Giraudon, and M. Berthod, "Information in Markov random fields and image redundancy," in *Selected Papers from the 4th Canadian Workshop on Information Theory and Applications II* (Springer-Verlag, 1996), pp. 250–268.
28. S. Geman and D. Geman, "Stochastic relaxation, Gibbs distributions, and the Bayesian restoration of images," IEEE Trans. Pattern Anal. Machine Intell. **PAMI-6**, 721–741 (1984).
29. B. E. A. Saleh and M. C. Teich, *Fundamentals of Photonics* (Wiley, 2007).
30. L. Mandel, "Sub-poissonian photon statistics in resonance fluorescence," Opt. Lett. **4**, 205–207 (1979).